2016 24th International Lightning Detection Conference &
6th International Lightning Meteorology Conference
18 - 21 April | San Diego, California, USA

Characteristics of the Two Active Stages of Lightning Activity in Hailstorms

Dong Zheng, Yijun Zhang
State Key Laboratory of Severe Weather
Chinese Academy of Meteorological Sciences
Beijing, China
zhd@camscma.cn

Shuang Xu, Yongqing Wang
School of Atmospheric Science
Nanjing University of Information Science & Technology
Nanjing, China

***Abstract*—Two hailstorms occurring in Beijing and Tianjin, respectively, are investigated on their lightning activities based on lightning data and structures based on radar data. Both hailstorms exhibited two lightning activity peaks: the first was before the hailfall occurred and the second was after the hailfall ended. The main polarity of the CG lightning was positive in the stage around the first peak and changed to be negative in the stage around the second peak. Both the hailstorms had stronger convections and the main positive charge regions at the middle levels during the first stage. Different from that the Beijing hailstorm experienced the enhancement of convection once again and formed the main positive charge at upper levels during the second stage, Tianjin hailstorm generated the second lightning frequency peak under the condition that the convection continued weakening and the main positive charge dropped to middle-low levels.**

Keywords—hailstorm; lightning activity; convection intensity

I. INTRODUCTION

Lightning activity in hailstorms is usually active. Besides, the lightning activity in hailstorms trend to have different characteristics from that in typical thunderstorms, and therefore may be used to identify and predict hailstorms. In contrast to typical thunderstorms, hailstorms generally feature much more frequent intra-cloud (IC) flashes and a greater proportion of positive cloud-to-ground (PCG) lightning.

Previous studies have noted that in some hailstorms there are two development stages, as defined by the lightning activity. For example, in the study of a hailstorm that occurred in Beijing on 31 May 2005, Zheng et al. (2009) reported that the hailstorm had two active stages of lightning activity, corresponding to the hailfall stage and post-hailfall stage. The first stage featured an inverted electric structure, while the second featured the usual tripole electric structure. The minimum value of lightning frequency between the two active stages corresponded to the end of the hailfall. In addition, the lightning frequencies during the second stage were much greater than those during the first. Wang et al. (2014) also reported two active stages of lightning discharge in a hailstorm over Guangdong on 17 April 2011, with the lightning frequency in the second stage being much higher than that in the first stage. Both of these studies showed that the lightning activity during the second stage was due to the re-enhancement of the dynamical and microphysical processes after their steady weakening during the hailfall.

This study analyzes the lightning activity of two hailstorms occurring in Beijing and Tianjin, respectively, and involved in the same weather system. In terms of lightning activity, the two hailstorms both showed two active stages characterized by distinct lightning frequency peaks, and the dominant CG lightning transformed from positive to negative. However, the two hailstorms exhibited notable differences in their electric structure and dynamical and microphysical processes.

II. DATA AND METHODOLOGY

A. Data

The data used in this study are as follows.

(1) SAFIR3000 (System d'Alerte Fondre par Interferometric Radioelecctrique 3000) three-dimensional lightning location system data: the SAFIR3000 system consists of one central station and three substations (the locations of the substations are shown in Fig. 1). The system locates the three-dimensional spatial positions of total lightning (IC lightning and CG lightning) radiation sources using interferometric technology at VHF frequencies from 110 to 118 MHZ and LF from 300 Hz to 3 MHz. The original lightning radiation sources are grouped into a lightning flash according to the following criteria: for IC lightning, the time interval and horizontal distance between adjacent radiation sources are less than 0.1 s and 7 km, respectively; for CG lightning, the values are 0.5 s and 7 km for adjacent return strokes, respectively; meanwhile, the duration of a lightning should be within 3 s. In this study, the SAFIR3000 system provided the total lightning data.

The positions of the lightning radiation sources are used to determine the location of the main positive charge region. A lightning flash starts from a strong electric field and develops bidirectional leaders with opposite polarity. Each leader spreads into the region of opposite polarity charge (MacGorman et al., 1981; Williams, 1985; Shao et al., 1996; Coleman et al., 2003). The negative breakdown at VHF band possesses higher energy, so it is more easily detectable (Shao et al., 1996; Rison et al., 1999; Thomas et al., 2001). Therefore, the area where radiation sources are concentrated is generally considered as the main positive charge region. The same method have been used in Zheng et al. (2009) and Liu et al. (2011) to deduce the main charge region based on the SAFIR data.

(2) CG lightning location system data: the CG lightning location system (LLS) in Beijing, Tianjin, and Hebei districts is part of the national CG lightning location network. It can provide the time, location, polarity, and intensity of a return strike. The criteria used to determine whether the strikes belong to the same CG lightning flash are as follows: the time interval between adjacent strikes is less than 0.5 s, and the horizontal distance is less than 10 km. In order to avoid the misidentification of IC to be PCG lightning, we use a 10 kA threshold suggested by Cummins et al. (1998) to discard the PCG lightning with peak current less than the threshold.

(3) Doppler radar data: The S-band Doppler weather radars used in this study (the locations are marked in Fig. 1) are located in the Tanggu district of Tianjin (39°02'38"N, 117°43'04"E) and Beijing (39°48'32"N, 116°28'19"E), respectively. The interval between adjacent volume scans is 6 min. For convenience of analysis, the reflectivity data were converted from the original polar coordinates to Cartesian coordinates and mosaic, to obtain data with 20 layers in the vertical with a 1-km interval, and a horizontal resolution of 1 × 1 km.

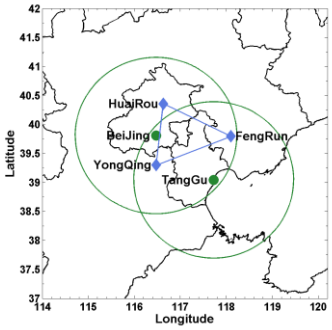

Figure 1. Locations of observational stations. (◆: Sub-station of the SAFIR 3000 three-dimensional lightning location system, ●: S-band Doppler radar. Circles denote the detection area of radar, within 150 km)

B. Methodology

(1) The definition of the hailstorm area: the hailstorms producing the hail are identified on the 3 km radar reflectivity image, according to the hail records from the meteorological department. The centers of radar reflectivity higher than 55 dBZ (the hailstorm in Beijing) and 45 dBZ (the hailstorm in Tianjin) are chosen as the center of a circle (taken as the core of the hailstorm), respectively. Smaller threshold for Tianjin hailstorm is attributed to that the radar reflectivity of the Tianjin hailstorm was relatively weaker than Beijing hailstorm. Next, a suitable circular region centered at the core is determined. The hailstorm body and the corresponding lightning activity within this region are analyzed. In determining the radius of the circular region, we considered the size of the hailstorm, the relationship of the hailstorm body with the surrounding clouds, the continuity of the spatial distributions of lightning activity, and the applicability of the radius during different stages. The value chosen for the radius of the Beijing hailstorm is 30 km during its most evolution but shrank to be 20 km during its decaying stage (corresponding to last five volume scans) in order to avoid the impact of a new cell. The radius for the Tianjin hailstorm is chosen as 20 km.

(2) Radar parameters: to facilitate an understanding of the evolution of the hailstorm structures, we use the following four radar parameters which were previously described by Yi et al. (2012).

Z_{max}: the maximum reflectivity (dBZ) at each level within the thunderstorm, which reflects the height of the strong core in the thunderstorm.

Z_{mean15}: the average value of the radar reflectivity $\geqslant$15 dBZ at each level within the thunderstorm, which reveals the development of the hailstorm and the number and distribution of ice particles within the cloud.

V_{40}: the volume of the radar echo $\geqslant$40 dBZ (km^3) within each level, which reflects the distribution of the strong echoes, and hence the scale and development of the thunderstorm.

The variability of the echo volume: the variation in the volume (km^3 per 6 min) of the 40 dBZ echo at a given time refers to the V_{40} value at this time minus the V_{40} at the previous scan time. This parameter provides information on the position and the variation of the strong core in a thunderstorm.

We define two additional parameters: $V_{40\text{-}Fup}$: the variation in V_{40} above –15 ℃ (km3 per 6 min). $V_{40\text{-}Fdown}$: the variation in V_{40} below –15 ℃ (km^3 per 6 min). According to the sounding data, the height of the –15 ℃ layer is ~6.58 km.

III. Analysis and Results

A. Evolution of the Thunderstorms

From 2100 BT (1300 UTC) to 2300 BT (1500 UTC) on 10 July 2007, a hail event in the Shunyi district of Beijing was recorded, with hail falling on Zhang Town, Yang Town, and 5 other towns and 76 villages. The hail started at 2200 BT (1400 UTC) and lasted for ~30 min, with the maximum diameter of hailstones being up to 6 cm. Another hail event was reported in Ji County of Tianjin on the same day. Here, the hail started at 2218 BT (1418 UTC) and lasted for ~12 min.

At 1230 UTC, a thunderstorm cell formed in northwestern Yanqing County. Thereafter, the radar echo began to strengthen and move to the southeast. At 1242 UTC, the thunderstorm cell moved to central Yanqing County, and another thunderstorm cell formed to the northeast of the first

cell. These two cells moved together, all the while moving closer to each other. At 1318 UTC, the two cells merged into a larger northeast–southwest-aligned thunderstorm cell (Beijing hailstorm) that started to move more slowly, with a radar echo intensity that reached 60 dBZ (Fig. 2a). At 1336 UTC, a thunderstorm cell was generated in the north of Ji County and moved southeast (Fig. 2b). At 1348 UTC, the Beijing hailstorm was located over Huairou and Miyun. The radar echo exhibited a typical bow shape, with echo intensity greater than 65 dBZ. A new thunderstorm cell formed to the southwest of the hailstorm in Tianjin. These two cells moved southeast and toward each other (Fig. 2c). At 1354 UTC, the two cells combined and formed a larger northeast–southwest-aligned thunderstorm cell (Tianjin hailstorm). The combined cell slowed down, while the intensity of its radar echo reached 60 dBZ (Fig. 2d). At 1400 UTC, hailstones were observed at the surface in the Beijing hailstorm. The northern part of the echo in Tianjin hailstorm weakened suddenly and then dissipated gradually. The southern part of the echo still moved southeastward (Fig. 2e). At 1406 UTC, the northern part of the Beijing hailstorm split into two. The western part continued to develop, while the eastern part began to weaken and gradually dissipated (Fig. 2f). At 1418 UTC, the western part of the Beijing hailstorm moved to Shunyi and strengthened again, with maximum reflectivity exceeding 70 dBZ. At the same time, the Tianjin hailstorm developed and strengthened, and the core of its radar echo reached 65 dBZ. The hail event began (Fig. 2g). After 1448 UTC, the Tianjin thunderstorm gradually weakened and split. After 1506 UTC, the Beijing hailstorm weakened and dissipated. At 1536 UTC, the Tianjin hailstorm cell also dissipated.

B. Lightning Activity and Electric Structure

Fig. 3 depicts the height distribution of the lightning radiation sources in the whole thunderstorm at every moment and temporal variations in the total lightning and the proportion of CG lightning. Next, we describe the Beijing and Tianjin hailstorms, respectively.

Overall, the Beijing hailstorm showed frequent total lightning activity with few CG lightning events (Fig. 3a). Over its lifetime, the maximum proportion of CG lightning was 13.3%, with an average of 0.91%. Based on the evolution of the total lightning activity and the hail event, the Beijing hailstorm could be divided into two active stages of lightning discharge characterized by two lightning frequency peaks; they corresponded to the hailfall stage (including the generation of the precipitable hailstone in cloud and its fall to the surface) and the post-hailfall stage (after the hailfall stopped). Before the hail event, the total lightning activity increased rapidly and reached a peak of 392 fl per 6 min at 1348 UTC. After that it began to decrease. At 1400 UTC, hail was observed. At the end of the hail event, the frequency of total lightning fell to its minimum value. Thereafter, it began to increase again and entered the second stage. At 1454 UTC, the frequency of total lightning reached its maximum (730 fl per 6 min). The lightning frequencies during the second stage were greater than those during the first stage. From the beginning to 1518 UTC (near the end of the rapid growth of total lightning in the second stage), the polarity of the CG lightning was always positive. Afterwards, negative CG lightning dominated.

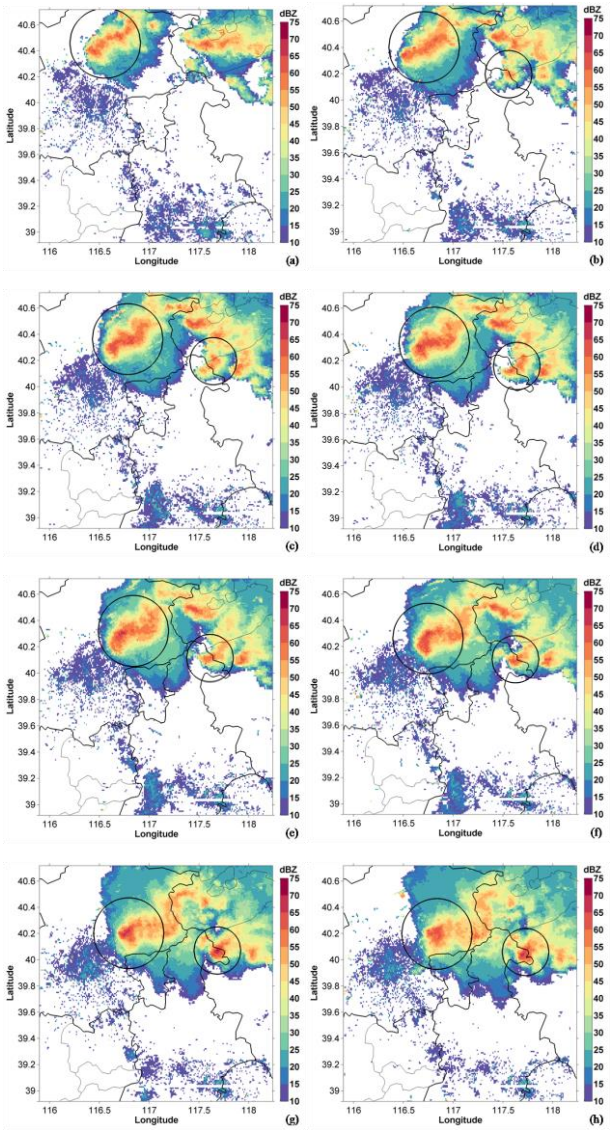

Figure 2. Radar composite reflectivity at (a) 1318 UTC, (b) 1336 UTC, (c) 1348 UTC, (d) 1354 UTC, (e) 1400 UTC, (f) 1406 UTC, (g) 1418 UTC and (h) 1424 UTC. (Hailstorm data are taken from the regions denoted by the circles)

According to the concept described in section II A, the area where radiation sources are concentrated is generally considered as the main positive charge region. In Fig. 3, the height of the main positive charge region varied considerably: in the initial stage (1236–1318 UTC), the center height increased from 6 to 7 km, and the corresponding temperature layer was between –10 and –20 ℃, which suggested an inverted electric structure. From 1324 UTC to 1354 UTC, the SAFIR data only had 2-D information, therefore, no height distribution of radiation sources were shown. From 1400 UTC to 1430 UTC, corresponding to the hail event, the maximum density of sources was centered at ~13 km. We speculate that the effect of subsidence of the hail led to the weakness of the middle charge and the transfer of the main discharge from middle levels to upper levels. After the hailfall, from 1436 UTC to 1554 UTC, the center of the main positive charge

increased from ~8 km to 11 km, which indicated a normal electric structure.

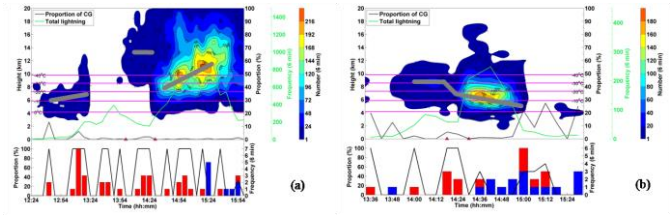

Figure 3. Time–height distribution of the lightning radiation sources in the whole chosen storms (color shading), and time series of total lightning frequency (green solid lines), the proportion of CG lightning (black dotted lines), the proportion of PCG lightning (black solid lines in the bottom figures), PCG lightning and NCG lightning frequencies (the red and blue bars, respectively, in the histograms) for Beijing hailstorm (a) and Tianjin hailstorm (b). The thick gray solid lines in the top figures represent the central positions of the main positive charge regions.

Fig. 3b shows that the Tianjin hailstorm also featured two stages in lightning activity. The maximum proportion of CG lightning was 27.3%, with an average of only 2.1%. At 1406 UTC, the total lightning reached the initial peak of 84 fl per 6 min. As the lightning activity declined, hailfall was observed. This declining trend lasted until the end of the hail event. This stage mainly featured PCG lightning. The proportion of PCG was as high as 87.5%, with only PCG lightning during most of the periods. After the hailfall, the lightning activity increased rapidly, reaching its maximum (248 fl per 6 min) at 1442 UTC. Subsequently the lightning activity weakened rapidly. Most of the CG lightning was negative, with the proportion of PCG lightning falling to 31.8%.

We infer from the height of the SAFIR radiation sources in Tianjin hailstorm that the main positive charge region centered at 8 km in the first stage, which suggested an inverted electric structure. When the hailfall occurred, the height of the positive charge region noticeably decreased. At the end of the hail event, the declining trend in height weakened and the main positive charge region centered at 7 km; that is, the electric structure kept inverted. In the second stage, the height of the center positive charge region continued to decline and varied at 6-7km when the frequency of lightning reached its peak; it seemed that the electric structure was still inverted while the positive charge region center middle-lower levels.

Comparing Fig. 3a and b, we conclude that the two hailstorms had the same characteristics of lightning activity. They both exhibited two active stages of lightning discharge. The polarity of the dominant CG lightning in the two stages was similar, and the relationships between lightning activity and the hail event were comparable. However, these two hailstorms exhibited notable differences in their electric structures during the second stage: the Beijing storm had normal electric structure with main positive charge being located at the upper level, and the Tianjin storm featured inverted electric structure with the main positive charge being located at middle-lower levels.

C. *Evolution of Structures of Storms*

Based on the radar reflectivity parameters (see section II B), the dynamics and the structure of precipitation are analyzed to explore the mechanism of the two active stages in hailstorms.

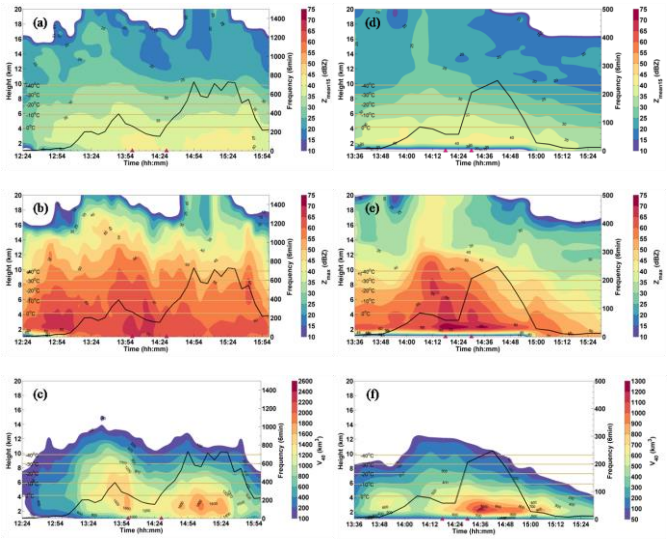

Figure 4. Time–height cross-sections (color shading) of (a, d) mean reflectivity (Z_{mean15}, dBZ), (b, e) maximum reflectivity (Z_{max}, dBZ), (c, f) 40 dBZ reflectivity echo volume (V_{40}, km^3), and time series of total lightning (black lines) for Beijing hailstorm (a–c) and Tianjin hailstorm (d–f).

Fig. 4 shows time–height cross-sections of the mean reflectivity (Z_{mean15}), the maximum reflectivity (Z_{max}), the 40 dBZ reflectivity echo volume (V_{40}), and the time series of total lightning. Initially, the profile of Z_{mean15} grew quickly (Fig. 4a) in the Beijing hailstorm. During the hailfall, the profile showed a declining trend. The average reflectivity below 4 km started to increase, which reveals that the number of large ice particles increased significantly at low levels. In the second active stage, the upper boundary of the profile of Z_{mean15} increased slowly, and generally remained steady during the period 1454–1530 UTC. Large average reflectivity appeared at low levels, corresponding to the heavy precipitation. The upper boundary of the profile of Z_{mean15} in the first stage was obviously higher than in the second active stage. Fig. 4b shows the peak value of lightning activity occurred around the maximum extension of Z_{max} in the vertical direction; the first stage featured the higher extension of Z_{max} relative to the second stage. Before the hail event, the value of V_{40} at each level increased significantly (Fig. 4c), indicating a rapid enlargement of the thunderstorm in the vertical direction. At the same time, the center of strongest V_{40} continuously moved downward. When the center of strongest V_{40} reached its lowest point (~3 km), the hail began to fall, followed by a rapid decrease in V40. In the second active stage, V_{40} increased again and the center of strongest V_{40} was maintained at 3 km. The maximum height of V_{40} and the speed of vertical expansion of V_{40} were both smaller than in the first stage.

In the Tianjin hailstorm, the profile of reflectivity $\geqslant$35 dBZ shows little change during 1342 1430 UTC (Fig. 4d). However, the profile of reflectivity <35 dBZ grew rapidly, reaching its peak value nearly simultaneously with lightning

activity. Subsequently (at 1436 UTC and later), the profile of reflectivity ⩽35 dBZ continued to decline until the end of the storm. Before hail was observed, large values of Z_{max} spread rapidly in the vertical direction (Fig. 4e), but then the center of strong Z_{max} moved down steadily. When it reached its lowest point, the hail event began. During the second stage, the vertical spread of Z_{max} continued to decrease. Fig. 4f shows that the center of strong V_{40} was at low levels, before the first peak of lightning, but afterwards it began to weaken. Before the hail event, V_{40} at all levels experienced rapid growth at the same time. After the hail event, the high values of V_{40} at low levels persisted or even increased, while values of V_{40} at high levels began to decrease.

In terms of their structure, the Beijing and Tianjin hailstorms have obvious similarities and differences. Before the hailfall, convection in both hailstorms was strong and reflectivity at all levels intensified markedly, indicating the growth of cloud particles at all heights. After the hailfall, the dragging effect of hailstones and the settlement of particles within the cloud led to the significant weakness of dynamic processes, and reflectivity at all levels weakened. However, in the second stage of frequent lightning discharges, their development characteristics are notably different. The convection of the Beijing hailstorm strengthened again, and the radar reflectivity apparently increased, although it was weaker than in the first stage. In contrast, the convection of the Tianjin hailstorm never recovered its strength, but the particles at middle-low level increased. For example, the radar parameters at high levels continued to decrease, and Z_{mean15} and V_{40} only remained and even strengthen at low levels.

To further understand the evolution of the thunderstorms at all levels and recognize the structure differences between the two hailstorms, we analyze $V_{40\text{-}Fup}$ and $V_{40\text{-}Fdown}$ (defined in section II B). The results are shown in Fig. 5.

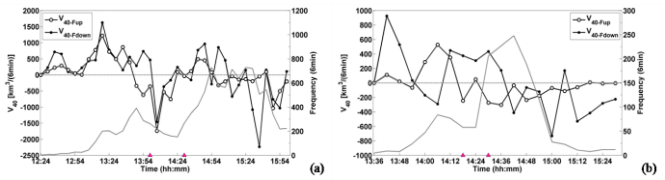

Figure 5. Time series of the radar parameters $V_{40\text{-}Fup}$ (km^3 per 6 min), $V_{40\text{-}Fdown}$ (km^3 per 6 min), and total lightning for Beijing hailstorm (a) and Tianjin hailstorm (b).

Before 1348 UTC of Beijing thunderstorm, $V_{40\text{-}Fup}$ and $V_{40\text{-}Fdown}$ were positive, which means that the storm strengthened rapidly. Accordingly, the total lightning peaked at 1348 UTC. From 1348 to 1400 UTC, $V_{40\text{-}Fup}$ dropped and became negative, while $V_{40\text{-}Fdown}$ remained positive, which shows that the hail particles was descending and the convective activity was reduced. At 1400 UTC, the hail event began. During the hailfall stage, both $V_{40\text{-}Fup}$ and $V_{40\text{-}Fdown}$ were negative and the thunderstorm weakened. At the same time, because of the fall of hailstones, ice particles decreased at all levels, as did the lightning activity. After the hail event (1430–1454 UTC), $V_{40\text{-}Fup}$ and $V_{40\text{-}Fdown}$ increased again and became positive as a result of strengthening of the thunderstorm. The corresponding lightning activity also increased and peaked at 1454 UTC. During 1500–1524 UTC, $V_{40\text{-}Fup}$ was slightly negative, while $V_{40\text{-}Fdown}$ fluctuated around zero, which indicated that ice particles above –15 ℃ weakened continually but slowly, while ice particles below –15 ℃ alternately increased and decreased. During this time, lightning activity was highly variable. During 1530–1600 UTC, the declining $V_{40\text{-}Fup}$ and $V_{40\text{-}Fdown}$ indicated that the thunderstorm was weakening, with a sharp reduction in lightning activity.

As for the Tianjin hailstorm, before the hail fell to the ground (1412 UTC), $V_{40\text{-}Fup}$ was positive, and $V_{40\text{-}Fdown}$ was mostly positive (Fig. 5b), indicating that the Tianjin thunderstorm was in a rapidly growing stage. Lightning activity reached its peak at 1406 UTC. In the subsequent period, $V_{40\text{-}Fup}$ fell below zero, indicating that the number of ice particles in the upper part of the thunderstorm was gradually reducing and that the intensity of the whole thunderstorm was weakening. However, during 1412–1436 UTC the positive $V_{40\text{-}Fdown}$ meant there was a rapid increase in hydrometeors in the middle-low part of the thunderstorm. Meanwhile, the main positive charge region was located at the –15 ℃ level and it decreased in height significantly. It is evident that the growth of ice particles at middle-low level contributed to the intense lightning activity. Thereafter, the total lightning reached a peak at 1442 UTC. After 1442 UTC, $V_{40\text{-}Fup}$ and $V_{40\text{-}Fdown}$ were both negative. The thunderstorm was in the weakening stage, with the lightning frequency decreasing rapidly.

To sum up, the volume change rates of reflectivity >40 dBZ show a good relationship to the enhancement and reduction of lighting activity. Especially in the Beijing hailstorm, the evolution of $V_{40\text{-}Fup}$ explains the change in lightning frequency. As for the Tianjin hailstorm, during the hail stage $V_{40\text{-}Fup}$ was closely related to lightning frequency, while in the second stage $V_{40\text{-}Fdown}$ had a stronger relationship to lightning frequency. The two active stages in the Beijing hailstorm corresponded to the two periods of enhanced convection (Fig. 5). In the Tianjin hailstorm, after the hail event the convection remained weak but still contributed to the second stage of active lightning. Similar results have not been reported previously. In addition, the thunderstorms strengthened rapidly before the hail event, with positive $V_{40\text{-}Fup}$. The peak of the total lightning activity before the onset of hailfall occurred approximately at the end of the rapid increase in $V4_{0\text{-}Fup}$. The hail occurred when $V_{40\text{-}Fdown}$ increased rapidly and just after $V_{40\text{-}Fup}$ became negative.

IV. DISCUSSION

A. *Relationship between Dynamical and Microphysical Processes and Electric Structure*

Here, the macroscopic development processes of the two hailstorms are discussed further, based on the above analysis. Initially, with strong dynamical processes, abundant water vapor was delivered upward and condensed (one of the necessary conditions for hail yield) in the Beijing hailstorm. In the presence of a high content of supercooled liquid water and according to the non-inductive charging (NIC) mechanism (Takahashi, 1978), large ice particles (e.g., graupel) carried a positive charge and small ice particles (e.g., ice crystals)

carried a negative charge in ice–ice rebound collisions in the mixed phase region. Eventually, a positive charge region formed at middle levels. The inverted-polarity charging under NIC mechanism was usually regarded to be responsible for the dominant inverted electric structure in severe thunderstorms (e.g., MacGroman et al., 2005; Tessendorf et al., 2007). During the hailfall, there was mainly downdraft in the storm, leading to an overall sharp decline of the thunderstorm. The original middle-level positive charge region probably weakened or even died away with the sedimentation of particles (Fig. 3a), the main discharge indicated by radiation sources transferred to the upper levels (Fig. 3a). After the hail, the thunderstorm strengthened again. According to the NIC mechanism, in the presence of suitable liquid water content above the reversal temperature level, graupel carries a negative charge and ice crystals carries a positive charge. Under the sustained action of the strong updraft, the charged region rose, resulting in the formation of the normal charge structure, with the main positive region located at the upper levels.

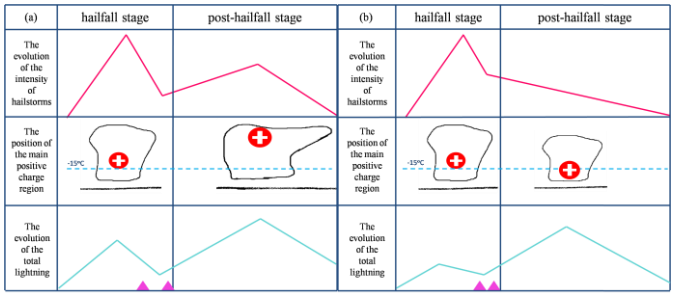

Figure 6. Conceptual graphs for the evolution of the storm intensity and electric structure for Beijing hailstorm (a) and Tianjin hailstorm (b).

The pre-hail process in the Tianjin hailstorm was similar to that in the Beijing hailstorm. Strong convection and high liquid water content contributed to an inverted charge structure. During the hail event, the downdraft caused the middle-level positive charge region to descend (Fig. 3b). However, because of the shorter and weaker hailfall, this positive charge region kept on existing and was involved in the dominant lightning discharges. More importantly, after the hail shooting, the convection continued to weaken. Though the height of this positive charge region decreased, its intensity increased. Referring to the analysis on Fig. 5b which indicates that the particles increased at the middle-low levels and decreased at the upper levels, we inferred that the possible reasons for the formation of the enhanced positive charge region under the weak convection are as follows. Many small ice particles remained at the middle and low levels after the first stage. Although the updraft was too weak to support vertical development of the thunderstorm, it ensured the maintenance of small ice particles at the middle and low levels and helped to generate more ice particles. At this time, most of the ice particles were located near but under –15 ℃ (the temperature inside the cloud is expected to be higher than this temperature), below the reversal temperature level. Under this condition, even if the original positive charge were not involved in the consideration, graupel would gain a positive charge in ice–ice collisions, thus further enhancing the positive charge. In summary, it was the reversed-polarity charging of the graupel under conditions of high liquid water content and low temperature that contributed to the frequent discharges in the first stage. The reversed-polarity charging of the graupel located below the reversal temperature level with suitable liquid water content contributed to the frequent discharges after the hail event.

Fig. 6 shows the evolutions of the two hailstorms and the position of the main positive charge region in the form of conceptual graphs, which might provide a simple but clear comparison between Beijing hailstorm and Tianjin hailstorm.

B. Dynamical and Microphysical Porcesses and Lightning Activity

Previous studies have assumed that lightning frequency and thunderstorm strength are strongly correlated. From a macro viewpoint, our research shows two exceptions to this assumption: (1) in the Beijing hailstorm, the convection was weaker in the second stage than in the first stage, but the lightning frequency was greater; (2) in the Tianjin hailstorm, there was more lightning activity although convection was weakened in the second stage. In the first stage, convection was strong before the hailfall. This process was possibly unfavorable for electrification, as the time-scale was too short to sustain the electrification and accumulate charge. In addition, the strong updraft would result in a short time for ice–ice collisions (under the action of the strong airflow, particles were expected to experience a quick rebound, so ice particles near the updrafts were unlikely to persist), and therefore a weak charging. An extreme example is the “lightning hole” observed above the main updraft of supercell (e.g., Krehbiel et al., 2000; Goodman et al., 2005). Finally, the growth of hailstones consumed large amounts of water vapor and prevented the formation of small ice particles. The concentration of large hail particles was low, and the integrated surface area was small, leading to hail particles carrying less charge. Under moderate convection, these unfavorable factors would be relatively weak or nonexistent. The electric structure of the second stage of the Tianjin hailstorm has already been discussed in section IV A.

In both Beijing and Tianjin hailstorms, the hail shooting occurred at surface after the peak of lightning activity. As mentioned above, when the hailstones were growing, the growth of the small ice particles was suppressed (with a larger density and greater integrated surface area), which is closely related to the process of electrification. Therefore, the lightning activity reached its peak before the hail fell to the ground. The interval between the peak in lightning frequency and the hail event might correspond to the time over which the hail further grew and then fell from the cloud to the ground.

V. CONCLUSTIONS

Based on the observation of SAFIR3000 and radars, this research examines the characteristics of lightning activity in a Beijing hailstorm and a Tianjin hailstorm, which occurred under the same weather conditions and within the same synoptic system. Both hailstorms had two stages of active lightning discharge: the hailfall stage dominated by PCG lightning and post-hailfall stage dominated by NCG lightning during its active period. The peak lightning frequencies in the

second stage were higher than those in the first stage. These results, combined with previous studies (Zheng et al., 2009; Wang et al., 2014), indicate that the occurrence of two stages of lightning activity in hailstorms might not be alone.

While the first active stage of lightning discharge associated with the hailfall events were both contributed by the strong convection, the second stage exhibited two different mechanisms: as for Beijing storm, the enhancement of the convection after the hailfall was responsible for the active lightning discharge in the second stage. However, the Tianjin storm experienced the more active lightning discharges in the second stage during its continuous weakening in convection intensity. Referencing to the evolution of radar data, it is speculated that the generation and aggregation of the particles at middle-low level under the action of the weak updraft strengthened the charging process, and caused the frequent lightning discharges.

Impacted by the strong dynamic processes in the storms, both Beijing and Tianjin hailstorms had inverted electric structures in the hailfall stage, which should be attributed to the inverted-polarity charging in the relatively cold levels (<–15^{o}C) with high liquid water content. In the post-hailfall stage, the Beijing storm finally formed normal electric structure because of the moderate convection and normal charging process. However, Tianjin storm kept its inverted electric structure in its post-hail fall stage, while the height of the positive charge decreased and there was inverted-polarity charging in the relatively warm levels (>–15^{o}C).

We deduced that the stronger convection and the generation of large-size particles in the hailfall stage was not in favour of the charging process (such as short time for ice–ice collisions and charge transfer and small integrated surface area for carrying charge), so the general lightning activity in the hailfall stage is weaker than that in the post-hailfall stage with relatively weak convection.

The rates of volume change of reflectivity >40 dBZ above and below the –15 ℃ level ($V_{40\text{-}Fup}$ and $V_{40\text{-}Fdown}$) showed a good relationship to the enhancement and decrease in lighting activity. The lightning peak corresponded to the peak stage of $V_{40\text{-}Fup}$ (i.e., the maximum rate of development in the upper part of the thunderstorm) or the stage when $V_{40\text{-}Fup}$ changed from positive to negative (i.e., when the upper part of a thunderstorm was strongest). The hailfall occurred when $V_{40\text{-}Fdown}$ increased rapidly and just after $V_{40\text{-}Fup}$ became negative.

ACKNOWLEDGMENT

This work was supported by National key fundamental research development program of 973 project (2014CB441402). Basic research projects of Chinese Academy of Meteorological Sciences (2014R017 and 2013Z006).

REFERENCES

Coleman, L. M., T. C. Marshall, M.Stolzenburg, T. Hamlin, P. R. Krehbiel, W. Rison, and R. J. Thomas (2003), Effects of charge and electrostatic potential on lightning propagation, *J.Geophys. Res.*, **108**, 4298.

Cummins, K. L., M. J. Murphy, E. A. Bardo, W. L. Hiscox, R. B Pyle, and A. E. Pifer (1998), A combined TOA/MDF technology upgrade of the U.S. National Lightning Detection Network, *J.Geophys. Res.*, **103**(D8), 9035–9044.

Goodman, S. J., and Coauthors (2005), The North Alabama lightning mapping array: recent severe storm observations and future prospects, *Atmos. Res.*, **76**, 423–437.

Krehbiel, P. R., Thomas R. J., Rison W, T. Hamlin, J. Harlin, and M. Davis (2000), GPS-based mapping system reveals lightning inside storms, *EOS Trans. Am. Geophys. Union*, **81**(3), 21–25.

Liu D., X. Qie, Y. Xiong, and G. Feng (2011), Evolution of the lightning activity in a leading-line and trailing stratiform mesoscale convective system over Beijing, *Adv. Atmos. Sci.*, **28**(4), 866–878.

MacGorman, D. R., A. A. Few, and T. L. Teer (1981), Layered lightning activity. *J.Geophys. Res.*, **86**, 9900–9910.

MacGorman, D. R., W. D. Rust, P. R. Krehbiel, W. Rison, E. Bruning, and K. Wiens (2005), The electrical structure of two supercell storms during STEPS, *Mon. Weather Rev.*, **113**, 2583–2607.

Rison, W., R. J. Thomas, P. R. Krehbiel, T. Hamlin, and J. Harlin (1999), A GPS-based three-dimensional lightning mapping system: Initial observations in central New Mexico, *Geophys. Res. Lett.*, **26**, 3573–3576.

Shao, X. M., and P. R. Krehbiel (1996), The spatial and temporal development of intracloud lightning, *J.Geophys. Res.*, **101**, 641–668.

Takahashi, T. (1978), Riming electrification as a charge generation mechanism in thunderstorms, *J. Atmos. Sci.*, **35**, 1536–1548.

Tessendorf, S. A., K. C. Wiens, and S. A. Rutledge (2007), Radar and lightning observations of the 3 June 2000 electrically inverted storm from STEPS, *Mon. Weather Rev.*, **135**, 3665–3681.

Thomas, R. J., P. R. Krehbiel, W. Rison, T. Hamlin, J. Harlin, D. Shown (2001), Observations of VHF source powers radiated by lightning, *Geophys. Res. Lett.*, **28**, 143–146.

Wang, C., D. Zheng, Y. Zhang, and L. Liu (2014), Lightning Activity and its relationship with the Storm Structure in a Hailstorm, *J. Trop. Meteor.*, **30**(6), 1127–1136 (in Chinese).

Williams, E. R. (1985), Electrical discharge propagation in and around space charge clouds, *J.Geophys. Res.*, **90**, 6059–6070.

Yi X., Y. Zhang, Y. Shen, and Y. Liu (2012), Observational analysis of a multicell hailstorm triggered by a sea-breeze front and its merging process, *ActaMeteor. Sinica*, **70**(5), 974–985 (in Chinese).

Zheng, D., Y. Zhang, Q. Meng, W. Lu, and X. Yi (2009), Total Lightning Characteristics and Electric Structure Evolution in a Hailstorm, *Acta. Meteor. Sinica*, (2), 233–249.